Effects of Large Polycyclic Aromatic Hydrocarbons on the Soot Formation in Ethylene-Air Nonpremixed Flames

S. Prabhu[1]*, P.G. Arias[1], Y. Wang[1], Y. Gao[2], S. Park[1], H.G. Im[1], S.M. Sarathy[1], S.H. Chung[1], T. Lu[2]

[1] Clean Combustion Research Center, King Abdullah University of Science and Technology, Thuwal, Saudi Arabia
[2] Department of Mechanical Engineering, University of Connecticut, Storrs, CT, USA

Abstract

This study presents updated comprehensive gas-phase kinetic mechanism and aerosol models to predict soot formation characteristics in ethylene-air nonpremixed flames. A main objective is to investigate the sensitivity of the soot formation rate to various chemical pathways for large polycyclic aromatic hydrocarbons (PAH). In this study, the detailed chemical mechanism was reduced from 397 to 99 species using directed relation graph (DRG) and sensitivity analysis. The method of moments with interpolative closure (MOMIC) was employed for the soot aerosol model. Counterflow nonpremixed flames of pure ethylene at low strain rate sooting conditions are considered, for which the sensitivity of soot formation characteristics with respect to hetrogeneous nucleation is investigated. Results show that higher PAH concentrations result in higher soot nucleation rate, and that the average size of the particles are in good agreement with experimental results. It is found that the nucleation processes (i.e., soot inception) from higher PAH precursors, coronene in particular, is critical for accurate prediction of the overall soot formation.

1. Introduction

Soot formation is an active field of combustion research, due to its significant health and environmental effects. Recently, the interest in soot models have expanded beyond only investigating the global soot properties, such as soot volume fraction and the particle size distribution, to include detailed chemical and physical pathways that lead to the formation and destruction of soot particles towards quantitative predictions at a wide range of flame conditions [1]. Today's advanced soot modeling involves two main components: (a) to describe the gas-phase chemistry involving polycyclic aromatic hydrocarbons (PAHs) that leads to soot particle nucleation; and (b) to model the subsequent particle growth and oxidation in a manner that reflects the associated physical heterogeneous processes.

Soot particle inception, or nucleation, is the initial formation of the smallest soot particles from gas-phase hydrocarbon molecules with a relatively lower molecular weight than the soot particles [2]. These smallest particles have sizes of the order of 1 nm and masses of about 1000 atomic mass units. Soot particle inception represents the path between the main gas-phase combustion chemistry and soot particle dynamics, and it determines the number of nascent soot particles in flames. Fuel decomposition and PAH growth pathways contribute to the formation and growth of aromatic species. The starting point for PAH growth is the formation of the first aromatic benzene ring, which is produced from the recombination of smaller aliphatics. These aliphatics are thus key contributors to soot formation, and include common combustion intermediates such as acetylene (C_2H_2), or propargyl radical (C_3H_3). After the formation of first ring aromatics, larger PAHs are formed through the "H-abstraction-C_2H_2-addition" (HACA) mechanism or via propargyl addition [3]. HACA is initiated by H-atom abstraction from the reacting aromatic molecules or other radicals, followed by the addition of an acetylene molecule to the radical site. At a certain size, PAH species begin to collide and stick to each other, while individual PAHs continue to increase in size via the HACA process. This combination of molecular chemical growth reactions and physical collisions leads to the appearance of soot particles [4-6].

Once initial soot particles are formed, physical collision processes between particles leads to the formation of larger soot particles. This process of soot particle coagulation occurs simultaneously with surface growth process. Unlike surface growth that changes the total mass of soot particles in flames, coagulation only changes the evolution of the soot particle size distribution. Particle coagulation is usually classified into two distinct processes: coalescent collision and agglomeration. In coalescent collision, two particles combine to form a single larger particle, while in agglomeration, two particles stick to form a chain-like structure with the identity of individual particles maintained [7,8]. Simultaneously with these growth processes, oxidation of the aromatics also occurs as a critical destruction pathway. The primary mechanism is believed to be free-edge oxidation of aromatics by oxygen molecules [9,10]. The oxidation by hydroxyl (OH) radical is unimportant at early stages of soot formation. However, the overall effects of PAH oxidation by O_2 on soot formation are twofold. On one hand, O_2 oxidizes and thereby suppresses carbon mass from participating in further growth reactions. On the other hand, O_2 promotes soot formation by building up the radical pool, especially H atoms for participating in HACA. Soot appearance is determined by the competition between soot formation and oxidation even at early stage of the process.

2. Model Description

2.1 *Gas-Phase Kinetic Mechanism*

Detailed chemical kinetic mechanisms describing the pyrolysis of hydrocarbon fuels and the formation of soot nucleating PAH species have been proposed by Frenklach and coworkers [5]. In addition, different approaches for modeling soot particle evolution under concurrent nucleation, coagulation, surface growth, and oxidation processes have also been developed. Models that rely on empirical inputs for soot nucleation, growth, and oxidation rates are inherently limited to specific conditions, and cannot be applied to conditions far from those under which the rates were measured. As such, they cannot be readily extended to different fuels or pressure conditions.

*Corresponding author: prabhu.selvaraj@kaust.edu.sa

$$r_{AB} = \frac{\max_i |\omega_i \delta_{Bi}|}{\max_i |V_{Ai} \omega_i|} \qquad (1)$$

$$\delta_{Bi} = \begin{cases} 1, & \text{if reaction involves B} \\ 0, & \text{otherwise} \end{cases}$$

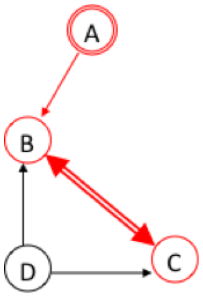

Figure 1: Directed Relation Graph. The importance of a species A with respect of B is described by a ratio of the importance of the reaction sensitivity.

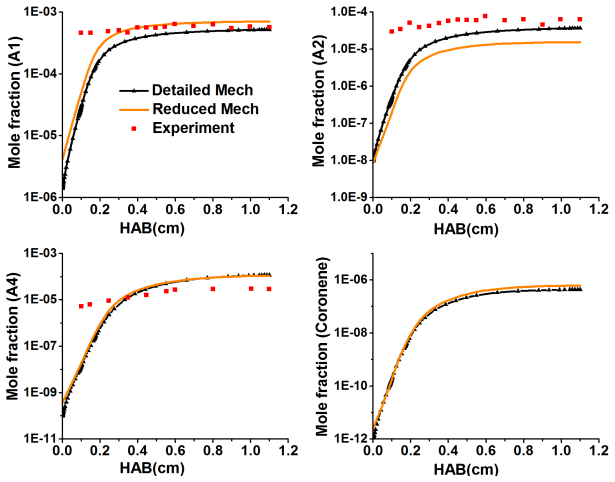

Figure 2: PAH species mole fraction profiles in premixed flames. Predictions using the detailed (line with symbols) and reduced (line) are compared with experimental measurements [12].

The present KAUST-Aramco PAH Mech 1.0 utilizes the comprehensively validated AramcoMech 1.3 $C_0 - C_2$ chemistry developed by NUIG, and extended up to benzene (C_6H_6 or A1). This mechanism contains accurate kinetic descriptions for the combustion of saturated and unsaturated hydrocarbons, namely methane, ethane, ethylene, and acetylene, and oxygenated species; formaldehyde, methanol, acetaldehyde, and ethanol [11]. The formation of aromatics larger than benzene were accounted by including the KAUST Mech 2 (KM2) PAH growth pathways up to coronene for the accurate prediction of soot formation [12]. A detailed chemical mechanism of 397 species that includes polycyclic aromatic hydrocarbons (PAH) up to coronene (A7) was reduced to 99 species using the directed relation graph technique (DRG) [13]. The resulting chemical mechanism is the latest in a series of mechanisms developed at KAUST with improved accuracy in predicting the formation of PAHs, which are important precursors for the growth of soot [14]. The reduction effort is the initial step to enable efficient direct numerical simulations of multi-dimensional turbulent reacting flows for improved understanding of turbulence-flame-soot interactions.

The method of DRG (Figure 1) is based on the observation that many species are only weakly coupled during combustion process, such that the species that do not significantly affect the reaction rates of the major species can be eliminated from the mechanism. Directed relation graph with expert knowledge (DRG-X) was used in the preliminary reduction of the mechanism [15]. The mechanism was reduced to 271 species (from the detailed 397 species) by assigning importance to PAH species. Additional reduction was accomplished using the sensitivity of each species and control over the error of the target parameters, which resulted in 99 species. Further computational cost savings is expected when additional reduction and stiffness removal is accomplished using quasi-steady state assumptions on fast chemical reaction steps.

The reduced mechanism was verified using CHEMKIN PRO for C_2H_4 premixed flames at atmospheric pressure and reactant fractions as $C_2H_4/O_2/N_2$ = 21.3/20.9/57.8 [12]. In Figure 2, the predictions of A1-A4 species mole fractions by the reduced mechanism agree well with those by the detailed mechanism, especially for the more important higher PAH species, and both modeling results show good agreement with experimental measurements.

2.2 *Simulation Configuration*

One-dimensional counterflow diffusion flame configuration is adopted for nonpremixed flame calculations. Following previous studies [16-18], Depending on the level of dilution in the fuel and oxidizer streams, the flame can be moved to the fuel side to establish a soot formation (SF) flame if located on the oxidizer side of a stagnation plane, such that the formed soot particles are convected toward the fuel stream without a subsequent soot oxidation process. A soot formation/oxidation (SFO) flame occurs when the flame is located on the fuel side such that soot particles are transported toward the high temperature oxidizer side. Due to oxidation, SFO flames demonstrate similar behavior to sooting premixed flames.

In the present study, the ethylene/air nonpremixed flame in SF configuration is considered at the atmospheric pressure condition. . A distance of 1.5 cm separates the fuel and oxidizer ports. The nozzle exit flow velocities for both the fuel and oxidizer streams were set at 13.16 cm/s and 16.12 cm/s. The oxidizer stream was composed of 25% O2 and 75% N2 by volume. The fuel stream was pure ethylene [19]. Computations are performed using the OPPDIF module of CHEMKIN [23]. For several representative cases, different grid parameters were tested to ensure grid convergence for all solutions reported in the following.

2.3 *Hetrogeneous Soot Model*

2.3.1 *Soot Nucleation*

The PAH-based soot model consists of various pathways including soot nucleation, surface growth through HACA/PAH condensation, particle-particle coagulation, and oxidation through chemical reactions. Soot particle aggregation is not considered and particles are assumed to be spherical. The inception of soot particles was carried out by eight different PAH molecules, through homogeneous as well as heterogeneous nucleation reactions. Homogeneous nucleation involves self-addition of PAHs, while heterogeneous nucleation involves addition of two different PAHs. A total of 36 nucleation reaction steps are considered and these reactions are assumed to be irreversible with zero activation energy. Each nucleation reaction rate is equal to the collision rate of the two precursors,

which is given by,

$$R_{ci} = \sum_{i=0}^{\infty}\sum_{j=0}^{\infty} \gamma * C_E * E_F * \sqrt{\frac{4\pi K_b T}{\mu_{i,j}}} * (D_i + D_j)^2 * C_i * C_j * N_a^2 \quad (2)$$

where D_i is collision diameter, C_i is concentration, C_E represents collision efficiency, E_F is Van der Waals factor, and γ is correction for collision efficiency. The collision efficiency represents the probability of successful creation of a new soot nucleus when two PAHs collide [16]. The correlation for the collision efficiency did not account for the dependence on temperatures, and is determined by [21]:

$$C_E = \frac{1}{1 + \exp\left[-2 * \left(\frac{D_{min}^3}{m_{min}} + \left(\frac{m_{min}}{1100}\right)^6 - 5\right)\right]} \quad (3)$$

where D_{min} and m_{min} are the collision diameter and mass of the smaller of the two colliding PAHs. The method of determining the correction constant, γ, required in the soot nucleation model is explained by Wang et.al [18], in which the baseline flame of pure C_2H_4 fuel was simulated by adjusting γ. It was shown that a satisfactory agreement between the simulated and experimentally observed maximum soot volume fraction was obtained with γ=0.0578.

2.3.2 *Condensation and Surface Growth*

Soot particle growth is described through surface reactions taking place on active sites. There are two types of surface sites involved in the model: (a) hydrogen sites where H atoms are bonded with carbon atoms, and (b) open sites indicating radical sites on dehydrogenated carbon atoms. These two types of sites are later referred to as H(se) and open(se), respectively. The overall site density (including H(se) and open(se)) was estimated to be 3.82E-9 mol/cm^2 and the soot bulk density was taken to be 1.8g/cm^3. This site density was used as a constant value, irrespective of the soot particle sizes. When a new soot nucleus is formed, its surface will be covered by H(se) and open(se). The total number density is fixed while the number of H(se) sites is determined by the number of H atoms during PAHs inception [18]. No gas-phase species will be generated in inception reactions. The number of open sites can then be calculated to balance the total number of surface sites.

2.3.3 *Oxidation*

Once soot particles are created in the flame zone, they start interacting with the surrounding gas mixture and with one another. If the oxidizers such as O, OH and O_2 are available in the gas mixture the soot particles are then subjected to oxidation. The most effective soot oxidizer in the flame zone is OH.

$$OH + open(se) + C(B) \Rightarrow CO + H(se) \quad (4)$$

As for the SF flames, the flame is present in the oxidizer side, and the particles travels towards the stagnation plane. In this scenario, there is no oxidation of soot particles due to the absence of oxygen and the rest of the oxidation is only due to the presence of OH.

2.3.4 *Soot Aerosol Model*

Soot predictions in terms of its number density, diameter, and volume fraction are governed in detail by the particle size distribution function (PSDF), which are represented by the method of moments with interpolative closure. Given a particle-size distribution function n(j), the r-th moment of the PSDF is defined as,

$$M_r = \int_0^{\infty} j^r * n(j) * dj \quad (5)$$

The particle tracking module uses the particle class, i.e., the number of bulk species molecules in the particle core, as the measure of particle size. The total mass of particle population is then calculated by

$$m_{p,\Sigma} = \sum_{j=0}^{\infty} (j * m_0) * N_j \quad (6)$$

where Nj is the discrete PSDF of size class j. The average particle diameter of the spherical particles can be given by

$$d_p = \frac{1}{N_\Sigma} \sum_{j=0}^{\infty} d_0 * j^{1/3} * N_j = d_0 * \frac{M_{1/3}}{M_0} \quad (7)$$

Since the HACA growth pathways and PAH condensation are surface processes, the total particle surface area A is an important parameter in determining the rates of these processes. The total sphere equivalent surface area of a particle population is given by

$$A_{s,\Sigma} = \sum_{j=0}^{\infty} A_{s,0} * j^{2/3} * N_j = A_{s,0} * M_{2/3} \quad (8)$$

A general definition of average diameters of the particle ensemble D_{pq} can then be written as,

$$D_{pq} = \left[\frac{\sum_{j=0}^{\infty} N(j).D(j)^p}{\sum_{j=0}^{\infty} N(j).D(j)^q}\right]^{\frac{1}{p-q}} \quad (9)$$

where D(j) is the diameter of particle with size class j.

$$\begin{aligned} D_{63} &= \left[\frac{\sum_{j=0}^{\infty} N(j).D(j)^6}{\sum_{j=0}^{\infty} N(j).D(j)^3}\right]^{\frac{1}{3}} \\ &= \left[\frac{\sum_{j=0}^{\infty} N(j).(d_0.j^{\frac{1}{3}})^6}{\sum_{j=0}^{\infty} N(j).(d_0.j^{\frac{1}{3}})^3}\right]^{\frac{1}{3}} = d_0.\left(\frac{M_2}{M_1}\right)^{1/3} \end{aligned} \quad (10)$$

where d_0 is the minimum diameter of the bulk core, corresponding to a single carbon atom. All of the three moments implicitly represent the shape of the PSDF. In this study, therefore, the transport equations of 3 moments (r = 0, 1 and 2) and surface species were coupled with the gas-phase continuity, momentum, energy and species equations to obtain chemical and soot structures of counterflow diffusion flames through the OPPDIF module of the Chemkin Pro package [23].

3. Results and Discussion

In Figure 2, it was confirmed that the detailed and reduced mechanisms predict PAH species in good agreement for premixed flames. Similar validations are now attempted for nonpremixed flames. Figure 3 shows the comparison of predicted PAH species profiles, A1, A2, A4 and coronene (A7), with experimental measurements by Wang et al. [9]. Although not shown here, the profiles of the main combustion products,

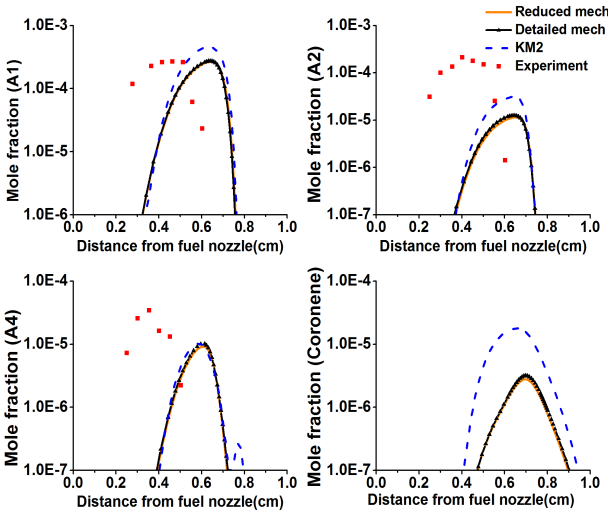

Figure 3: PAH mole fraction profiles in counterflow diffusion flame. Predictions using the detailed (dotted line with symbols), reduced (line), and earlier KM2 (dash-dot line) mechanisms are compared with experimental measurements [9].

such as CO_2, CO, and H_2O, are all found to be accurately predicted.

In addition to the detailed and reduced mechanisms employed in the present study, calculations using the KM2 mechanism [9] are also shown for comparison. The new (detailed and reduced) mechanisms show good agreement with each other, while some discrepancies are observed in comparison with the predictions by the KM2 mechanism. In particular, about an order of magnitude differences in the coronene mole fraction are observed. Unfortunately, no experimental data were available for this quantity, so it is unclear to judge which prediction is more accurate.

Next, detailed investigations are conducted to identify the contributions of various pathways to the overall soot mass growth rate. Figure 4 shows the predictions using the detailed (dotted line with symbols) and reduced (solid line) mechanisms for the contributions of the nucleation, HACA surface growth, PAH condensation, respectively, to the net soot growth rate profiles. The net effect on the particle number density prediction is also shown. The overall qualitative behavior in terms of the peak location and the width of the profiles is found to be consistent between different reaction mechanisms. For example, the HACA surface growth rate reaches a maximum at a region near 0.72 cm, which coincides with the C_2H_2 concentration peak at a distance of 0.65 cm combined with the temperature effect. In comparison, the surface growth rate due to PAH condensation occurs in a slightly wider region with a peak closer to the fuel side as expected. In contrast to the remarkably good agreement in the PAH concentration predictions by the detailed and reduced mechanisms (Figure 3), Figure 4 shows that there are noticeable differences in the predictions of the surface growth rate by all individual pathways. The nucleation surface reaction involves 8 PAH species, in which gas phase species such as benzo(a)pyrene, benzo(e)pyrene are under predicted and this results in a difference in reduced mechanism. Thus the nucleation surface reaction will result in hydrogen open site, which involved in HACA growth path. As a result HACA growth rate was reduced with the reduced mechanism. This reduction in particle growth rate subsequently leads to the same level of differences in the net prediction in the soot volume fraction, as will be discussed later.

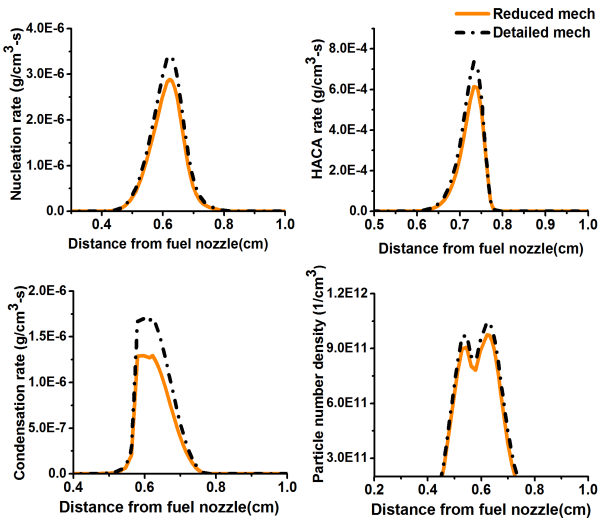

Figure 4: Predictions of various pathways contributing to the soot particle growth rates & Particle number density

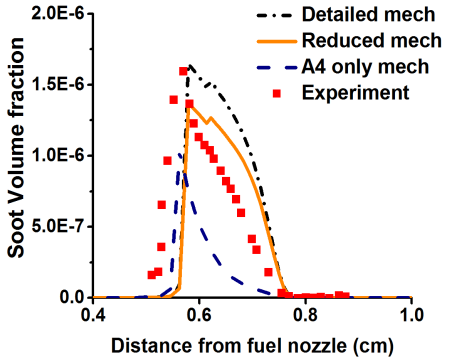

Figure 5: Soot volume fraction profiles predicted by the detailed (dash-dot line with symbols), reduced (solid line), A4-only (dashed line) mechanisms compared with the experimental data.

The present reaction mechanism considered detailed nucleation pathways involving PAHs up to A7, while most previous detailed reaction mechanism considered up to A4. To assess the significance of the additional pathways contributed by A5-A7, a contrived numerical experiment was conducted by truncating all gas-phase nucleation reactions including A5-A7. This case is referred to as "A4-only" reaction mechanism. Figure 5 shows the comparison of the soot volume fraction profiles predicted by the detailed, reduced, and A4-only mechanisms. The differences between the detailed and reduced mechanism results reflect the observation in Figure 4. Both results, however, show good agreement with the experimental measurements within a reasonable margin of uncertainties. On the other hand, the A4-only mechanism yields a significantly underpredicted soot volume fraction. The main difference is attributed primarily to the contributions from the PAH condensation, which is significantly enhanced in the presence of larger PAH molecules. In Figure 6, the computed D_{63} was derived from the ratio of the second to the first moment, which implicates the similarities of average diameter predictions

remains the same with reduced and detailed mechanism. As the diameter D_{63} from computed moments, are predicted because there is no assumption of size distribution function, whereas in the experiments it is attributed to the self similar particle size distribution.

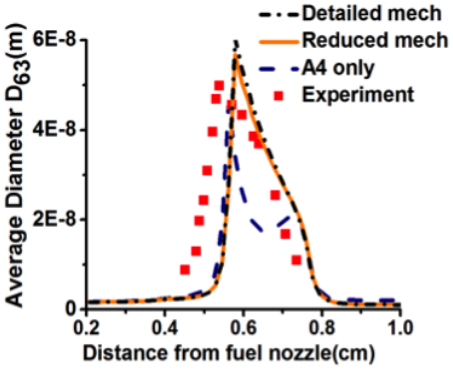

Figure 6: Average particle Diameter profiles predicted by the detailed (dash-dot line), reduced (solid line), A4-only (dashed line) mechanisms compared with the experimental data [18].

Finally, it is noted that the effect of the oxidation reactions to the soot growth process was found to be negligible in the present study, which is expected considering the SF flame configuration. Future work will investigate the effects of the oxidation reactions on the net soot formation of SFO flames.

4. Conclusions

This study developed an updated detailed and reduced kinetic mechanism for soot formation in ethylene flames and then reduced the mechanism to predict the soot formation in counterflow diffusion flames. Experimentally measured PAH concentrations in premixed flames were well predicted by the reduced mechanism. Simulation results of soot volume fraction of the counterflow flames showed good agreement with the experimental results. A sensitivity analysis confirmed the impact of larger PAH species (especially coronene) in the heterogeneous nucleation process, leading to a significant quantitative difference in the prediction of the soot volume fraction. In order to extend the study on the sensitivities of larger soot particles, it is important to consider the morphology of the soot and also the effect of condensation pathway.

Acknowledgements

This work was sponsored by King Abdullah University of Science and Technology.

References

[1] A.Z. Mansurov, Combustion, Explosion and Shock Waves. 41 (2005) 727-744.

[2] M. Frenklach and H. Wang, Combust. Flame. 23 (1990) 1559-1566.

[3] A. Raj, M.J. Al Rashidi, S.H. Chung, S.M. Sarathy, J. Phys. Chem. A 118 (2014) 2865-2885.

[4] M. Frenklach, H. Wang, Detailed mechanism and modeling of soot particle formation, Springer-Verlag, New York, NY, 1994.

[5] J. Appel, H. Bockhorn, M. Frenklach, Combust. Flame, 121 (2006) 122-136.

[6] I. Kennedy, Prog. Energy Combust. Sci., 23 (1997) 95-132.

[7] Q. Zhang, H. Guo, F. Liu, G.J. Smallwood, M.J. Thomson, Proc. Combust. Inst., 32 (2009) 761-768.

[8] S.H. Park, S.N. Rogak, W.K. Bushe, J.Z. Wen, M.J. Thomson, Combust. Theor. Model. 9 (2005) 499-513.

[9] A. Raj, G.R. da Silva, S.H. Chung, Combust. Flame. 159 (2012) 3423-3436.

[10] A. Raj, S.Y. Yang, D. Cha, R. Toyouo, S.H. Chung, Combust. Flame. 160 (2013) 1812-1826.

[11] W.K. Metcalfe, S.M. Burke, S.S. Ahmed, H.J. Curran, Int. J. Chem. Kinet. 45 (2013) 638-675.

[12] Y. Wang, A. Raj, S.H. Chung, Combust. Flame. 160 (2013) 1667-1676.

[13] T. Lu, C.K. Law, Proc. Combust. Inst., 30 (2005) 1333-1341.

[14] S. Dworkin, Q. Zhang, Combust. Flame. 158 (2011) 1682-1695.

[15] T. Lu, M. Plomer, Z. Luo, 7th US National Combustion Meeting (2011) RK38.

[16] J. Y. Hwang, S. H. Chung, Combust. Flame. 125 (2001) 752-762.

[17] B. C. Choi, S. K. Choi, S. H. Chung, Proc. Combust. Inst. 33 (2013) 609-616.

[18] Y. Wang, A. Raj, S.H. Chung, Combust. Flame., in press. doi:10.1016/j.combustflame.2014.08.016.

[19] A. Raj, M. Sander, V. Janardhanan, M. Kraft, Combust. Flame. 157 (2010) 523-534.

[20] N.A. Slavinskaya, U. Riedel, S.B. Dworkin, M.J. Thomson, Combust. Flame 159 (2012) 979-995.

[21] A. Violi, A. D'Anna, A. D'Alessio, A.F. Sarofim, Chemosphere 51(2003) 1047-1054.

[22] V. Chernov, M.J. Thomson, S.B. Dworkin, N.A. Slavinskaya, U.Riedel, Combust. Flame. 161 (2012) 592-601.

[23] Chemkin Pro: a chemical kinetics package for the analysis of gas-phase chemical kinetics, Reaction Desig, Release 15112. 2011.